Nanotechnology

International Edition: DOI: 10.1002/anie.201501060
German Edition: DOI: 10.1002/ange.201501060

An Organic Microlaser Array Based on a Lateral Microcavity of a Single J-aggregation Microbelt**

*Qing Liao, Xue Jin, Haihua Zhang, Zhenzhen Xu, Jiannian Yao, and Hongbing Fu**

Abstract: *A laser array on the nano- and microscale is a key component for integration in photonic devices, but remains a challenge when using semiconductor nanowire lasers. Here we report a low-threshold lateral-cavity microlaser, formed between two lateral-faces of a single-crystalline organic microbelt (OMB) of 1,4-dimethoxy-2,5-di-[4′-(cyano)styryl]benzene (COPV). By cutting a single OMB into six pieces by a top-down two-photon processing technique, we successfully fabricated a compact and uniform 1×6 microlaser array along the length direction of the OMB. The microlasers had excellent reproducibility and addressable high precision, thus making them attractive candidates as miniaturized coherent light sources for future nanophotonics.*

During the past decade, semiconductor nanowire nanolasers have been the topic of intensive investigation as a result of their applications, such as for on-chip optical communication,[1] logic nanophotonics,[2] high-throughput sensing,[3] and ultrahigh-resolution imaging.[4] For practical use, the alignment and orientation of nanowire lasers are crucially important for integration into devices.[5] Although there is a remarkable maturity in the synthesis of complex nanowire structures,[6,7] the integration of high-density and highly uniform nanowire laser arrays still remains a critical challenge.[8] The reasons are: 1) as the axial Fabry–Pérot (FP) waveguide modes are sensitive to morphological factors of the nanowires, the lasing properties of each single nanowire laser in the array, such as cavity modes, lasing threshold, etc., are difficult to exactly reproduce. 2) Post-synthesis assembly techniques for nanowire integration, such as electric- or magnetic-field assisted alignment,[9,10] optical tweezers,[11] and laminar flow in microfluidic channels,[12] are not low cost and still do not achieve a high yield and good reproducibility with high precision.

Organic semiconductors are of current interest in photonic applications because of their large optical cross-sections (absorption, emission, etc.) and broad spectral tunability.[13] Moreover, the self-assembly of organic molecules provides a powerful tool to generate complex nanostructures driven by weak intermolecular interactions of the van der Waals type.[14] For example, organic nanowires can be readily prepared by the self-assembly of planar π-conjugated molecules, thereby enabling the realization of high-performance field-effect transistors (FETs),[15] optical waveguides,[16] and optically pumped lasers.[17] As organic molecules are highly anisotropic, it is widely accepted that the molecular packing arrangement in the solid state has a significant effect on the physicochemical properties and, furthermore, the performances of the corresponding devices.[18] Therefore, understanding the influence of the molecular arrangement on the optical confinement effect in the solid state is important for developing novel organic photonic devices.

Herein, we report FP-cavity microlasers formed between two lateral faces of single-crystalline organic microbelts (OMBs) of 1,4-dimethoxy-2,5-di[4′-(cyano)styryl]benzene (COPV), which are completely different from previously reported axial FP cavities formed between two end faces of nanowires.[19] We found that alignment of COPV molecules nearly parallel to the direction of the belt length generates photoluminescence (PL) light perpendicular to the direction of the belt width. Thus, the PL undergoes reflections back and forth between two lateral faces, such as inside a FP cavity. Moreover, this brickwork molecular arrangement also leads to highly emissive J-aggregates with a quantum yield of $\Phi > 0.58 \pm 0.04$.[20] Single and multiple mode lasing from the OMB lateral cavities were observed as a function of the belt width (W) around 2–8 μm, shorter than the length of nanowire lasers (at least 10 μm).[19] By cutting a single OMB into six pieces with a top-down two-photon processing technique, we fabricated a compact and uniform 1×6 microlaser array.

In our experiments, regularly shaped OMBs of COPV were prepared by a modified self-assembly method in solution.[19,21] In a typical synthesis, 100 μL of a stock solution of COPV (5 mM) in tetrahydrofuran was injected into 2.0 mL of hexane under stirring. Figure 1a presents a scanning electron microscopy (SEM) image of typical products obtained after aging for 24 h. It can be seen that the COPV OMBs are highly faceted with a uniform width (W) of 1–10 μm along the entire length (L) of several tens of micrometers. The thickness is around 300–600 nm according to atomic force microscopy measurements. The top inset of Figure 1a shows the selected-area electron diffraction

[*] Dr. Q. Liao, X. Jin, H. H. Zhang, Dr. Z. Z. Xu, Prof. H. B. Fu
Beijing Key Laboratory for Optical Materials and Photonic Devices
Department of Chemistry, Capital Normal University
Beijing 100048 (People's Republic of China)
Prof. J. N. Yao, Prof. H. B. Fu
Beijing National Laboratory for Molecular Sciences (BNLMS)
Institute of Chemistry, Chinese Academy of Sciences
Beijing 100190 (People's Republic of China)
E-mail: hongbing.fu@iccas.ac.cn
Prof. J. N. Yao, Prof. H. B. Fu
Collaborative Innovation Center of Chemical Science and Engineering, Tianjin 300072 (People's Republic of China)

[**] This work was supported by the National Natural Science Foundation of China (Nos. 91222203, 21273251, 91333111, 21190034, 21221002) and the National Basic Research Program of China (973) (2011CB808402, 2013CB933500).

Supporting information for this article is available on the WWW under http://dx.doi.org/10.1002/anie.201501060.

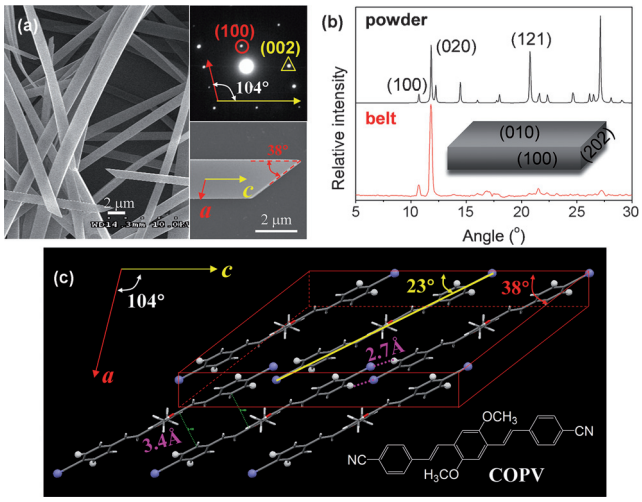

Figure 1. a) Typical SEM image of COPV OMBs. Top inset: SAED pattern. Bottom inset: high-magnification SEM image. b) XRD spectrum of a mat of COPV OMBs on a silicon wafer (bottom red line). For comparison, the simulated powder pattern based on single-crystal data is also included (top line). The inset shows a schematic representation of a COPV OMB. c) Brickwork molecular arrangement viewed perpendicular to the top face of the OMB.

(SAED) pattern, which could be identified and indexed to a monoclinic COPV crystal (CCDC no. 838078)[21] with cell parameters of $a = 8.5110(15)$ Å, $b = 14.954(3)$ Å, $c = 8.4748(15)$ Å, $\alpha = \gamma = 90°$, $\beta = 104.292°$. The SAED spots in a circle and triangle (top inset of Figure 1a) are due to (001) and (200) Bragg reflections with lattice spacing (d) values of $d_{(001)} = 8.4$ Å and $d_{(200)} = 4.2$ Å, respectively, and $\measuredangle$-(001)/(200) = 104°. X-ray diffraction (XRD) analyses (Figure 1b) also showed that the XRD peaks observed for the OMBs can be perfectly indexed to the single-crystal data and are dominated by the (020) peak. The correlation of the SEAD and XRD results suggests that the COPV OMBs are single crystals that preferentially grow along the crystal [001] direction. The inset of Figure 1b shows a schematic representation of a COPV OMB, bounded by (010) and $(0\bar{1}0)$ crystal planes on the top and bottom faces, (100) and $(\bar{1}00)$ crystal planes on the two lateral faces, $(\bar{2}02)$ and (202) crystal planes on the two end faces. Note that $\measuredangle$(100)/(202) = 38° could be clearly observed from a single OMB shown in the bottom inset of Figure 1a.

Figure 1c depicts the molecular arrangement within the crystal *ac* plane. It can be seen that COPV molecules are packed in a brickwork arrangement through π-π stacking (3.4 Å, see green dashed lines in Figure 1c) and hydrogen-bonding interactions [the distance between the phenyl hydrogen atoms C(7 A)-H and the cyano nitrogen N(1) atoms is 2.7 Å, see pink dashed lines in Figure 1c]. The COPV molecules are tilted at an angle of 23° to the lateral faces of the OMB and an angle of 12° to the substrate, therefore, almost parallel to the length direction of the OMBs. This is quite different from previously reported organic nanowires, in which π-conjugated molecules are generally perpendicular to the length direction of the nanowires to maximize π-π interactions.[15–17,19]

As we previously reported, the brickwork arrangement of COPV molecules leads to J-type aggregation in the solid state.[20,21] The absorption and PL spectra of the COPV monomers in dilute solution are broad and structureless with maxima at $\lambda_{abs,monomer} = 413$ nm ($\varepsilon_{monomer} = 58\,300\ M^{-1}cm^{-1}$) and $\lambda_{PL,monomer} = 474$ nm, respectively. In sharp contrast, J-aggregates of CPOV exhibit bathochromically shifted and unusually narrow absorption ($\lambda_{abs,J} = 482$ nm, $\varepsilon_J = 84\,500\ M^{-1}cm^{-1}$) and PL ($\lambda_{PL,J} = 491$ nm) bands (Figure S1). As the Stokes shift of COPV J-aggregates is as small as 380 cm^{-1}, self-absorption takes place in OMBs and results in the 0–1 emission at 520 nm being much stronger than the 0–0 emission at 491 nm (see the inset of Figure 2a). In any event, single-crystalline J-aggregate OMBs of COPV are highly emissive, with a value of $\Phi > 0.58 \pm 0.04$, higher than that of nanoparticles.[20]

We investigated individual single OMBs using a micro-PL system,[19,21] by focusing (with a 50×0.9 NA objective) the second harmonic ($\lambda = 400$ nm, pulse width 150 fs) of a Ti:sapphire regenerative amplifier to a 40 μm diameter spot to uniformly excite the isolated single belt (Scheme S1). Neutral density filters were used to change the power density of the excitation. Micro-PL spectra were collected by using a 3D movable objective coupled to an optical fiber and detected using a liquid nitrogen cooled charge-coupled device (CCD). A cut-off filter at 490 nm was used to eliminate the 400 nm excitation light.

Figure 2a summarizes the PL spectra of a single OMB with $W = 2.2$ μm and $L = 60$ μm (as shown in Figure 2b) at different excitation intensities. At a low pump density of $P = 0.83\ \mu J\,cm^{-2}$ (blue line), PL from 500 to 550 nm was assigned to the 0–1 band arising from spontaneous emission. When the pump density exceeds a threshold, from $P = 1.01\ \mu J\,cm^{-2}$ (red line) to $1.29\ \mu J\,cm^{-2}$ (black line), a strong laser emission developed as a pair of sharp bands at 522 and 533.5 nm. The linewidth of the individual lasing peaks is about 0.6 nm, much narrower than the full width at half maximum (FWHM = 22 nm) of the 0–1 spontaneous emission band below the threshold. Figure 2h shows a plot of the integrated PL intensities of the 0–1 band as a function of pump density (P), and clearly shows a lasing threshold at $P_{th} = 1.09\ \mu J\,cm^{-2}$. The intensity dependence can be fitted to a power law x^p with $p = 0.48 \pm 0.02$ below the threshold and $p = 2.78 \pm 0.08$ above the threshold, thus indicating a transition from a sublinear regime that is dominated by bimolecular quenching to a superlinear regime.[22]

The PL lifetimes were measured with a streak camera (Figure 2f). At $P = 0.1\ P_{th}$, the PL follows single exponential decay with a time constant of 0.33 ± 0.02 ns, in good agreement with that of nanoparticles.[20] Upon increasing the pump intensity to $P = 0.75\ P_{th}$, biexponential PL decay takes place with the short component ascribed to the bimolecular quenching.[22] Above the threshold, for example, at $P = 1.55\ P_{th}$, the PL decay time collapses to < 10 ps and is limited by the resolution of our experimental apparatus. The short PL lifetime above the threshold is a result of effective stimulated emission process.

Figure 2c,d displays the corresponding micro-PL images of the 2.2 μm OMB recorded below and above the threshold, respectively. Below the threshold, homogeneous PL was

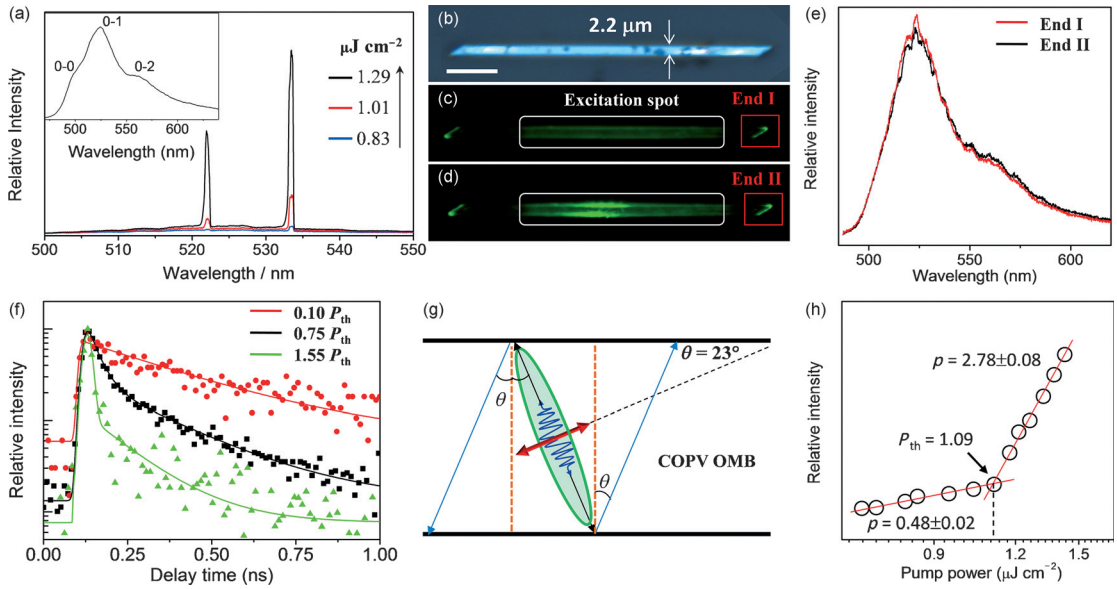

Figure 2. a) PL spectra of an OMB with $W = 2.2$ μm as a function of excitation density, recorded at the excitation point. The inset shows the absorption spectra of a mat of COPV OMBs on a quartz plate. b) The bright-field micrograph of this 2.2 μm OMB and (c,d) corresponding PL micrographs recorded below and above the lasing threshold, respectively. The scale bar is 10 μm. e) The PL spectra recorded at the end position as labeled by the red square in (c,d) under $P = 0.75\ P_{th}$ (black) and $P = 1.55\ P_{th}$ (red), respectively, are almost the same. f) PL decay curves monitored at 533.5 nm using a streak camera under different excitation dennsities. g) Schematic representation to elucidate the influence of molecular orientation on the formation of the FP cavity between two OMB lateral faces. h) Power-dependence profile of integrated PL intensities of the 0–1 peak recorded at the excitation point.

observed within the 40 μm excitation region (white rectangle in Figure 2c); above the threshold, very bright PL spots were observed near the center of the excitation region at both lateral sides of the 2.2 μm OMB (Figure 2d). This is different from nanowire lasers, which exhibit bright PL spots at both ends above the threshold as a result of its axial FP cavity.[19] Therefore, in our case, it is the two lateral faces of the OMBs that function as two reflectors to form a FP cavity. PL spots coupled at two OMB ends showed similar brightness below and above the threshold, as marked by the red squares in Figure 2c,d. It can be seen from Figure 2e that the PL spectra recorded at the OMB end are almost identical below and above the lasing threshold, similar to the spontaneous emission.

A schematic representation is shown in Figure 2g to illustrate the origin of the lateral FP cavity formed in the OMBs. As mentioned above, the COPV molecules (red double-arrow in Figure 2g) stack nearly parallel to the length of the OMB, tilted at an angle of 23° with respect to the lateral faces. It is known that the transition dipole of COPV is along the molecular long axis.[20] Therefore, PL light emitted by the COPV molecules is mainly within a plane perpendicular to its transition dipole (see the green oval in Figure 2g), and is also perpendicular to the length of the OMBs. Significant light leakage would take place at the interface between the bottom face of the OMB and the quartz substrate. However, reflections of PL light between two lateral faces are highly possible and lead to a FP cavity along the direction of the belt width.

Figure 3c–e displays the effect of the cavity size of three individual OMBs with $W = 3.1$, 5.4, and 8.2 μm, respectively. We fitted the PL spectrum to a sum of Lorentzian peaks and

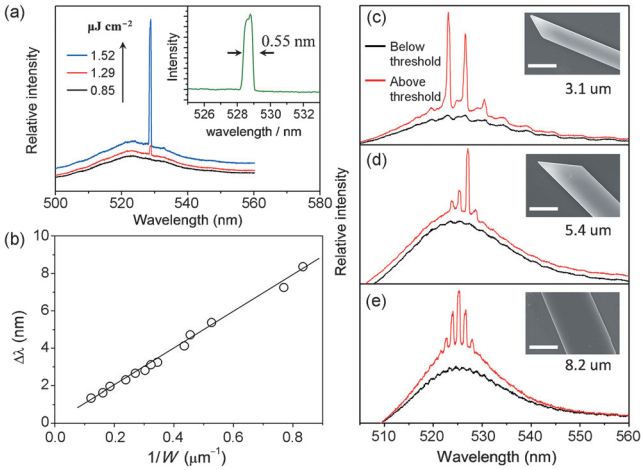

Figure 3. a) Single-mode lasing spectra from an OMB with $W = 1.6$ μm. The inset shows that the linewidth of the single-mode lasing peak is 0.55 nm. b) Plot of the mode spacing $\Delta\lambda$ at 520 nm as a function of $1/W$. c–e) High-resolution PL spectra below (black) and above (red) the threshold for OMBs with $W = 3.1$, 5.4, and 8.0 μm, respectively. The insets show high-magnification SEM images of the corresponding OMBs. Scale bars are 5 μm.

extracted the mode spacing ($\Delta\lambda$) at 520 nm in each case. According to the equation of the mode spacing for a FP cavity,[19] $\Delta\lambda = (\lambda^2/2W)[n - \lambda(dn/d\lambda)]^{-1}$, where n is the phase refractive index and $dn/d\lambda$ the dispersion relation, we plotted $\Delta\lambda$ as a function of $1/W$ in Figure 3b. The approximately linear relationship between $\Delta\lambda$ and $1/W$ confirms that the pair of optically flat lateral faces of an OMB can function as two reflectors and form an FP microcavity along its width.

Compared with multimode lasing, single-mode lasing is more attractive due to the absence of mode competition and the excellent monochromic properties of the laser beam.[23] In principle, once the mode spacing $\Delta\lambda$ is larger than the material gain width, single mode lasing would be possible.[23] Figure 3a shows the PL spectra of an isolated OMB with $W =$ 1.6 μm under different pump energy intensities. At low pump density, the PL spectrum is dominated by the broad spontaneous emission showing a mode spacing $\Delta\lambda = 5.6$ nm (Figure 3a, black line), which matches well with the $\Delta\lambda \approx 1/W$ fitting linear curve in Figure 3b. As the pump energy intensity increased above the lasing threshold, a single-mode lasing peak appears at 531 nm. The threshold of single mode lasing in a 1.6 μm wide OMB was found to be larger than that of multimode lasing observed in wider OMBs. We calculated the cavity quality factor (Q) according to the equation $Q = \lambda/\delta\lambda$, where λ is the wavelength of the peak and $\delta\lambda$ is the FWHM of the peak below the threshold.[24] Based on the data in Figure 3a,c–e, the Q value was found to increase as the width of the OMBs increased, and $Q = 102$, 306, 568, and 868 were obtained for OMBs with $W = 1.6$, 3.1, 5.4, and 8.2 μm, respectively.

"Soft" organic semiconductor nanostructures are compatible with sub-micrometer patterning and electromagnetic confinement within subwavelength volumes. For example, Pisignano and co-workers demonstrated the enhancement of polymeric fiber forward emission by imprinting periodic nanostructures using room-temperature nanoimprint lithography.[25] Based on the peculiar property of the lateral-cavity lasing of COPV OMBs, we fabricated a compact microlaser array by means of a top-down two-photon processing (TPP) approach. In brief, a near-infrared femtosecond laser [$\lambda =$ 800 nm, pulse width of 100 fs, 1 kHz) from a Ti:sapphire regenerative amplifier laser system (Spectra Physics)] was focused using a cylindrical lens into a rectangular shape of 1 cm in length and about 1 μm in width.[26] The OMBs on the substrate were scanned at an optimized speed by a step motor controlled by a computer and were cut by femtosecond pulses with a wavelength of 800 nm.

Figure 4a shows a 1×6 microlaser array fabricated using TPP on a single COPV OMB. Each subunit has a length of about 10 μm and a width of $W = 3.0$ μm, exactly the same as that defined by the original OMB. We characterized the lasing performances of each single subunit by focusing the 400 nm 150 fs excitation light into a spot of approximately 10 μm. The characteristic lasing spectra obtained from each subunit are shown in Figure 4c. It is clear that all these spectra have the same lasing modes. Furthermore, similar lasing threshold values can be observed (Figure 4d). Finally, we extended the size of the focusing point of the 400 nm excitation light to about 60 μm. Figure 4b demonstrates that the six subunit microlasers in the array can operate simultaneously at a pump density of 1.5 μJ cm^{-2}, which is above the lasing thresholds of each subunit (see Figure 4d). Remarkably, the microlaser array can be irradiated by a 400 nm excitation laser above the threshold for over 2000 s and their PL intensity shows no apparent fatigue (Figure 4e). This indicates the high stability and uniformity of our microlaser array.

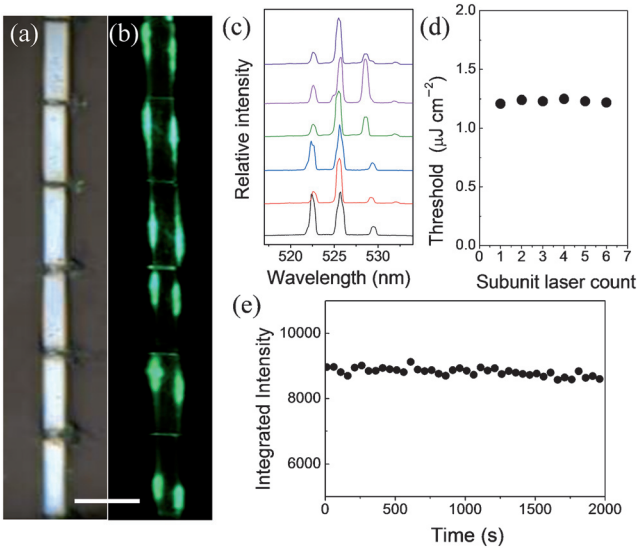

Figure 4. a) The bright-field image of a microlaser array. b) PL image of the corresponding array on excitation at 400 nm above the lasing threshold. The scale bar is 10 μm. c,d) PL spectra and threshold values from the different subunits. e) The lasing emission intensities as a function of 400 nm laser irradiation time.

In conclusion, we demonstrated the first low-threshold lateral-cavity microlaser based on single-crystalline OMBs of COPV. Single and multiple mode lasing from the OMB lateral cavities were observed as a function of the belt width (W) of around 2–8 μm. By means of a top-down two-photon processing approach, we successfully fabricated a compact uniform 1×6 microlaser array with good reproducibility and addressable high precision. We demonstrated that six subunit microlasers in an array can operate simultaneously with good stability. These features make our microlaser array attractive as a coherent light source for miniaturized photonic circuits.

Keywords: laser array · nanostructures · nanotechnology · photochemistry · photonic devices

How to cite: *Angew. Chem. Int. Ed.* **2015**, *54*, 7037–7041
Angew. Chem. **2015**, *127*, 7143–7147

[1] B. Piccione, C. H. Cho, L. K. van Vugt, R. Agarwal, *Nat. Nanotechnol.* **2012**, *7*, 640.
[2] H. Wei, Z. Wang, X. Tian, M. Kall, H. Xu, *Nat. Commun.* **2011**, *2*, 387.
[3] M. Law, D. J. Sirbuly, J. C. Johnson, J. Goldberger, R. J. Saykally, P. D. Yang, *Science* **2004**, *305*, 1269.
[4] F. Qian, Y. Li, S. Gradecak, H. G. Park, Y. Dong, Y. Ding, Z. L. Wang, C. M. Lieber, *Nat. Mater.* **2008**, *7*, 701.
[5] R. F. Service, *Science* **2010**, *328*, 810.
[6] B. Tian, P. Xie, T. J. Kempa, D. C. Bell, C. M. Lieber, *Nat. Nanotechnol.* **2009**, *4*, 824.
[7] P. Caroff, K. A. Dick, J. Johansson, M. E. Messing, K. Deppert, L. Samuelson, *Nat. Nanotechnol.* **2009**, *4*, 50.
[8] E. M. Freer, O. Grachev, X. Duan, S. Martin, D. P. Stumbo, *Nat. Nanotechnol.* **2010**, *5*, 525.
[9] P. A. Smith, C. D. Nordquist, T. N. Jackson, T. S. Mayer, B. R. Martin, J. Mbindyo, T. E. Mallouk, *Appl. Phys. Lett.* **2000**, *77*, 1399.

[10] Y. Li, F. Qian, J. Xiang, C. M. Lieber, *Mater. Today* **2006**, *9*, 18.
[11] A. Jamshidi, P. J. Pauzauskie, P. J. Schuck, A. T. Ohta, P.-Y. Chiou, J. Chou, P. Yang, M. C. Wu, *Nat. Photonics* **2008**, *2*, 86.
[12] Y. Huang, X. Duan, Q. Wei, C. M. Lieber, *Science* **2001**, *291*, 630.
[13] S. Chénais, S. Forget, *Polym. Int.* **2012**, *61*, 390.
[14] F. J. M. Hoeben, P. Jonkheijm, E. W. Meijer, A. P. H. J. Schenning, *Chem. Rev.* **2005**, *105*, 1491.
[15] K. H. Kim, S. Y. Bae, Y. S. Kim, J. A. Hur, M. H. Hoang, T. W. Lee, M. J. Cho, Y. Kim, M. Kim, J. I. Jin, S. J. Kim, K. Lee, S. J. Lee, D. H. Choi, *Adv. Mater.* **2011**, *23*, 3095.
[16] N. Chandrasekhar, R. Chandrasekar, *Angew. Chem. Int. Ed.* **2012**, *51*, 3556; *Angew. Chem.* **2012**, *124*, 3616.
[17] S. Varghese, S. J. Yoon, E. M. Calzado, S. Casado, P. G. Boj, M. A. Díaz-García, R. Resel, R. Fischer, B. Milián-Medina, R. Wannemacher, S. Y. Park, J. Gierschner, *Adv. Mater.* **2012**, *24*, 6473.
[18] C. Park, J. E. Park, H. C. Choi, *Acc. Chem. Res.* **2014**, *47*, 2353.
[19] Z. Xu, Q. Liao, Q. Shi, H. Zhang, J. Yao, H. Fu, *Adv. Mater.* **2012**, *24*, OP216.
[20] Z. Xu, Q. Liao, Y. Wu, W. Ren, W. Li, L. Liu, S. Wang, Z. Gu, H. Zhang, H. Fu, *J. Mater. Chem.* **2012**, *22*, 17737.
[21] Q. Kong, Q. Liao, Z. Xu, X. Wang, J. Yao, H. Fu, *J. Am. Chem. Soc.* **2014**, *136*, 2382.
[22] S. Kéna-Cohen, S. R. Forrest, *Nat. Photonics* **2010**, *4*, 371.
[23] X. Wang, Q. Liao, Q. Kong, Y. Zhang, Z. Xu, X. Lu, H. Fu, *Angew. Chem. Int. Ed.* **2014**, *53*, 5863; *Angew. Chem.* **2014**, *126*, 5973.
[24] Z. Xu, Q. Liao, X. Wang, H. Fu, *Adv. Opt. Mater.* **2014**, *2*, 1160.
[25] F. Di Benedetto, A. Camposeo, S. Pagliara, E. Mele, L. Persano, R. Stabile, R. Cingolani, D. Pisignano, *Nat. Nanotechnol.* **2008**, *3*, 614.
[26] L. Wang, Q. D. Chen, R. Yang, B. B. Xu, H. Y. Wang, H. Yang, C. S. Huo, H. B. Sun, H. L. Tu, *Appl. Phys. Lett.* **2014**, *104*, 031904.

Received: February 4, 2015
Published online: April 27, 2015

